Experimental study of the cyclic visco-elasto-plastic behaviour of a polyamide fibre strap

Guilhem Bles, Wojciech Nowacki, Ali Tourabi

Experimental study of the cyclic visco-elasto-plastic behaviour of a polyamide fibre strap

G. Bles[a]*, W. K. Nowacki[b], A. Tourabi[c]

17 January 2009

(a) – Laboratory LBMS - ENSTA Bretagne/Brest University/ENIB, Engineering School Ensta Bretagne (MSN), 2 rue François Verny, F-29806 Brest cedex 9, France.
(b) – Institute of Fundamental Technological Research, ul. Świetokrzyska 21, 00-49 Warsaw, Poland.
(c) – Laboratory 3SR, Domaine Universitaire, B.P. n^{o}53, F-38041 Grenoble cedex 9, France.

Abstract

Experimental tensile tests were performed on polyamide-based (PA66) woven strap samples. A strain measuring device was used to measure the strain in the middle and effective part of the woven tensile sample. The tests were performed, on the one hand under monotonous tension at different strain rates and on the other hand under sophisticated cyclic loading histories, including relaxation and creep sequences. The analysis of experimental results was made through a visco-elasto-hysteresis model, based on the superimposition of three stress components. The proposed method allows for characterizing the steady state viscous stress as a function of strain and strain rate, the time-independent irreversible behaviour and the instantaneous modulus increasing with the strain. Based on the visco-elasto-hysteresis model, an analysis enabled us to understand and predict the change in relaxation and creep orientations during complex loading histories.

Keywords: Polymers, Fibres, Ropes, Viscoelastic, Nonlinear elasticity, Relaxation, Creep.

1 Introduction

A polyamide 6-6 (PA66) fibre strap is used as a mechanical component for the parachute ejection of heavy cargoes from the hold of a plane in flight. The parachute is first ejected from the hold, while the cargo is still in the plane. The wind inflates the parachute, which then pulls the cargo out of the hold. The straps studied are the mechanical link between the parachute and the cargo. A plane crash may occur if a strap fails during the ejection phase. To address this risk and predict the mechanical performance of the straps, the definition of an effective modeling of mechanical behaviour of straps is required.

This mechanical structure is woven with polymer fibres. Many authors are working towards modeling the mechanical phenomena which occur within the weave at a mesoscopic level. Models were proposed for fabrics: fabric lattice model (Kato et al., 1999), mesostructurally based continuum model (King et al., 2005), material model for weave fabric (Pargana et al., 2007). Other authors proposed to describe the mesostructure of ropes (Leech, 2002), and proposed models for the mechanical behaviour of ropes based on their mesostructure (Beltran and Williamson, 2005; Ghoreishi et al., 2007).

The results of this type of studies, on two-dimensional (fabrics) or one-dimensional structures (ropes), are very interesting in order to understand the deformation mechanisms at the mesoscale level within the weave and their influence on the macroscopic behaviour. But in general, they ignored a great part of behaviour, which includes intricate time-dependent phenomena.

*Corresponding author. Tel.: +33 298 34 8913; fax: +33 298 34 8730; email: guilhem.bles@ensta-bretagne.fr

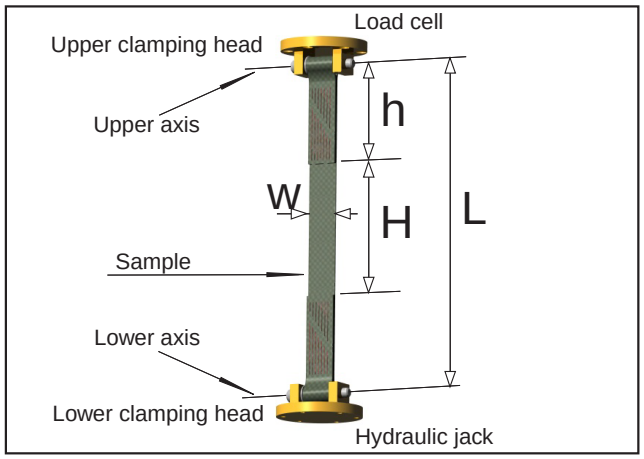

Figure 1: Measurements of polyamide strap attached to hydraulic testing machine.

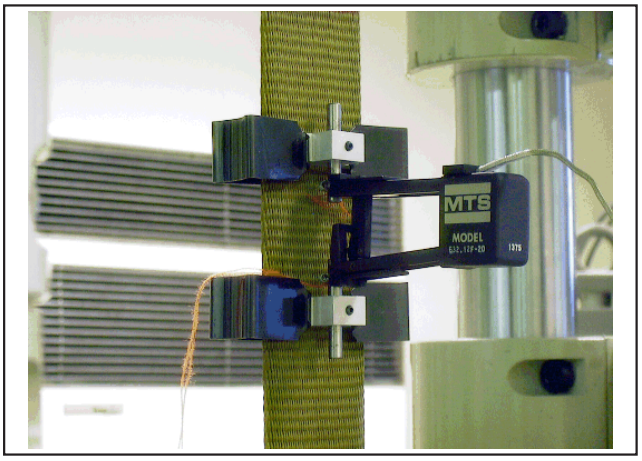

Figure 2: Strain measuring device for the woven strap in its effective area.

Phenomenological approaches and macroscopic continuum models are another way to model the mechanical behaviour of woven materials. In this framework, some authors proposed models based on anisotropic formulation (Holzapfel et al., 2001; Xue et al., 2003; Baesu, 2007).
Experimental investigations were also conducted on one-dimensional structures like mooring lines for offshore applications (Banfield and Casey, 1998; Fernandes and Rossi, 2005) or energy absorber ropes for worker security (Spierings and Stämpfli, 2006).
But, little research deals with the visco-elasto-plastic behaviour of polymer fibres, in order to analyse the reversible and irreversible phenomena that occur simultaneously during complex loadings. However, we may refer to the experimental work reported in Averett et al. (2006), which studied the effect of uniaxial cyclic loading on the mechanical behaviour of a nylon fibre.

The aim of the present study was to discern and to characterize the essential generic aspects of the behaviour of PA66 straps, starting with the stress-strain-time experimental measurements. For this purpose, monotonous tensile, cyclic tensile loadings with creep and relaxation periods were performed at various constant strain and stress rates. The characterization work was based on a macroscopic approach, through phenomenological description of the behaviour, using a visco-elasto-hysteresis constitutive model (Bles et al., 2000a), in the one-dimensional case. An identification method of the theoretical model parameters is proposed. All the aspects concerning the complete modeling of cyclic behaviour of straps were excluded from the scope of this study, which was limited to the experimental aspects. However, the results of identification method allow to describe partially the behaviour of the straps, by pointing out essential features like steady state viscous stress, time-independent behaviour or instantaneous modulus.

2 Experimental techniques

These structural components were manufactured by weaving polyamide 6-6 (PA66) strands, a semi-crystalline polymer. Three sets of polyamide strap were tested, called here A, B and C. Each sample is identified by a three-character code: ANM, BNM or CNM. Where A, B or C are for the strap groups, and the last two characters NM correspond to two sequence numbers. The present paper deals mainly with the set of A and B sample groups, but some results concerning the group C are presented here.

The polyamide strap has end-connections made by two sewn loops (fig. 1). The length of the central or effective part is about three times the width of the strap. The initial measurement of the samples (sewing length, axis distance etc.) was taken for each strap. The mean values and standard deviations of geometrical parameters described in figure 1, are indicated with the confidence interval *c.i.* of 95%:

$L = 491,0 \pm 0,5\ mm$, $H = 149,5 \pm 0,7\ mm$, $h = 171,2 \pm 0,5\ mm$ $(95\%\, c.i.,\ n = 40)$.

The stress applied to the woven sample was calculated from the load measure according to the assumptions of continuum mechanics. The woven strap was assumed to be an homogeneous continuum. The tensile stress was calculated as the Piola-Kirchhoff-1 stress $\sigma = F/S$ and $\dot{\sigma} = \dot{F}\ /S$, where F is the applied load and $S = 152 \pm 6\ mm^2$ is the cross section of the sample.

An experimental device was developed in order to adapt a standard extensometer to get a strain measure of the woven material (fig. 2). Two sets of pairs of metallic parts grip the strap on two sections, by means of four clips (black parts in fig. 2). Two needles are placed through each pair of metallic parts and go through the weaving. The needles ensure that the strap is well gripped by the device and avoid any sliding during the test. The device is put on the sample with a gauge part, so the initial length is reproductible. The strain and strain rate of the strap are defined as $\varepsilon = \Delta b/b_0$ and $\dot{\varepsilon} = \dot{\Delta b}\ /b_0$, with $\Delta b = b - b_0$ denotes the variation of distance measured by the extensometer during the mechanical tests and bo the initial length.

3 Theoretical pattern to analyse the experimental results

A modeling approach at the macroscopic level is adopted in order to predict the cyclic thermomechanical behaviour of a wide range of solid materials (Tourabi et al., 1995, 1997; Bles et al., 2000a). According to a phenomenological view, this modeling approach discerns the essential physical phenomena and superimposes them so as to predict the global macroscopic behaviour (Bles et al., 2002).

In the present case of polyamide straps, our approach consisted of the superimposition of three stress components corresponding to a nonlinear viscoelastic, a nonlinear elastic and a pure hysteresis behaviour. Many authors developed visco-elasto-plastic models (Frank and Brockman, 2001; Lubarda et al., 2003; Lin and Schomburg, 2003; Drozdov and Christiansen, 2006) and some of them have adopted the stress superimposition principle, like Miehe and Keck (2000) and Mulliken and Boyce (2006) in the case of rubbery and glassy polymers. Our approach will be described by section 3.1 in a one-dimensional case. In section 3.2, the main properties of the visco-elasto-hysteresis model (stemming from this phenomenological approach) are presented.

3.1 Fundamental superimposition assumption and visco-elasto-hysteresis model

The fundamental superimposition assumption was inspired by Duhem's method (Duhem, 1980). According to this assumption, the stress applied to the material is the result of a superimposition of several stress components. Each of these constitutive stresses is related to a physical phenomenon that occurs during mechanical loading. As regards the strain, it is left whole, without splitting up. To model the *visco-elasto-plastic* mechanical behaviour of the present PA66 straps, we considered the superimposition of three stress components $\sigma_h(\varepsilon, \xi)$, $\sigma_r(\varepsilon)$ and $\sigma_v(\varepsilon, \dot{\varepsilon})$:

$$\sigma(\varepsilon, \dot{\varepsilon}, \xi) = \sigma_h(\varepsilon, \xi) + \sigma_r(\varepsilon) + \sigma_v(\varepsilon, \dot{\varepsilon}) \tag{1}$$

where each stress component is defined by a specific constitutive equation, in a differential form.

As the three stresses are equal to zero at the initial mechanical state of material:

$$\sigma(\varepsilon = 0, \dot{\varepsilon}, \xi) = \sigma_h(\varepsilon = 0, \xi) = \sigma_r(\varepsilon = 0) = \sigma_v(\varepsilon = 0, \dot{\varepsilon}) = 0 \tag{2}$$

The stress component $\sigma_h(\varepsilon, \xi)$ is elastoplastic and always irreversible; it is a function of the current strain ε and of its history denoted here by the parameter ξ. The stress component $\sigma_r(\varepsilon)$ is nonlinear elastic. The stress component $\sigma_v(\varepsilon, \dot{\varepsilon})$ is viscoelastic with a nonlinear viscosity as this stress has a nonlinear relation with the strain rate $\dot{\varepsilon}$ and is also a function of the strain ε. Figure 3 illustrates this assumption, proposing a *visco-elasto-hysteresis* pattern of a phenomenological modeling. Each stress component is presented by a symbolic model. Its mechanical behaviour is qualitatively illustrated

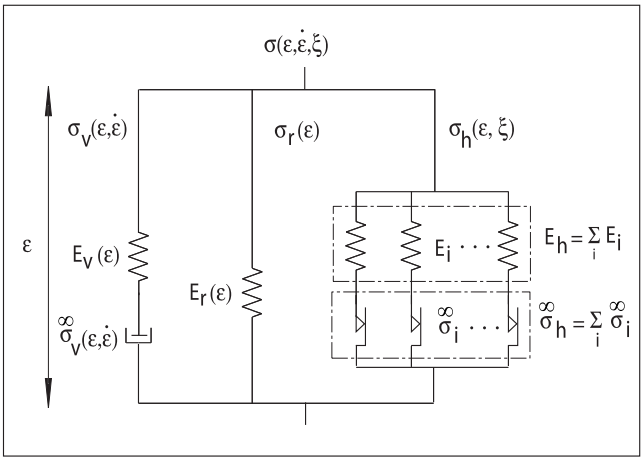

Figure 3: Visco-elasto-hysteresis behaviour model in the one-dimensional case.

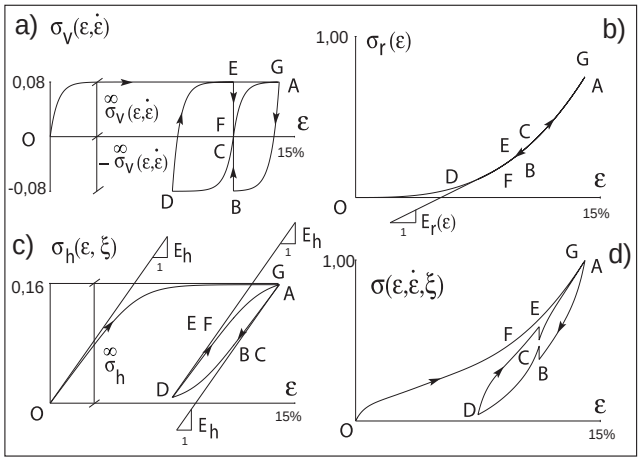

Figure 4: Cyclic behaviour of the three stress components of the visco-elasto-hysteresis model.

Table 1: Definition of the reference states during the loading $OADA$ on figure 4c.

branch	ξ	reference state	$\widehat{\varepsilon}\,(\xi)$	$\widehat{\sigma}_h(\xi)$
OA	0	origin O	0	0
AD	1	reversal point A	ε_A	$\sigma_h(\varepsilon_A, 1)$
DA	2	reversal point D	ε_D	$\sigma_h(\varepsilon_D, 2)$

in figure 4; with the proportion of each component $\sigma_v(\varepsilon, \dot{\varepsilon})$, $\sigma_r(\varepsilon)$, $\sigma_h(\varepsilon, \xi)$ and with the total stress $\sigma(\varepsilon, \dot{\varepsilon}, \xi)$. This figure shows that the result of the stress superimposition presents the typical *bean* shape of the stress-strain cycles often observed with materials woven in polymer fibres.

The pure hysteresis component $\sigma_h(\varepsilon, \xi)$ models the rate-independent irreversibilities of the mechanical behaviour. That part of the behaviour is called *equilibrium hysteresis* by Lion (1997) about the behaviour of rubbers. The related physical phenomena are of dry friction type and occur at the microscopic level in the crystalline phase of the fibres and/or at the mesoscopic level due to the interactions between yarns. Figure 4d illustrates the effect of the stress component $\sigma_h(\varepsilon, \xi)$, which makes the C and F points different at the end of BC and EF relaxation periods. In the case of viscoelastic behaviour, these ends of relaxation periods are coincident (fig. 4a). The main parameters of the behaviour of the stress component $\sigma_h(\varepsilon, \xi)$ are an elastic modulus E_h and a plastic yield stress $\overset{\infty}{\sigma}_h$ (fig.3 and 4c). The whole behaviour curve is divided into different loading or unloading branches (like OA, AD or DA on figure 4c), where the stress increases or decreases but always monotonously. Each branch of loading or unloading starts from a reference state memorized by $\widehat{\varepsilon}\,(\xi)$ and $\widehat{\sigma}_h(\xi)$ at the origin of the graph (point O) or at *reversal* points (points A and D fig. 4c). The parameter ξ is the result of a specific numbering of the reference states and is used to define the stress difference $\Delta\sigma_h(\varepsilon, \xi) = \sigma_h(\varepsilon, \xi) - \widehat{\sigma}_h(\xi)$ and strain difference $\Delta\varepsilon(\varepsilon, \xi) = \varepsilon - \widehat{\varepsilon}\,(\xi)$, where:

$$\frac{d}{dt}\,\widehat{\varepsilon}\,(\xi) \;\equiv\; \frac{d}{dt}\,\widehat{\sigma}_h(\xi) \equiv 0 \qquad\qquad \forall\xi \tag{3}$$

Consequently, the rates of $\Delta\sigma_h(\varepsilon, \xi)$ and $\Delta\varepsilon(\varepsilon, \xi)$ are identical to the current rates $\dot{\varepsilon}$ and $\dot{\sigma}_h\ (\varepsilon, \xi)$ respectively. Table 1 defines the parameter ξ, the successive reference states, $\widehat{\varepsilon}\,(\xi)$ and $\widehat{\sigma}_h(\xi)$ during the loading $OADA$ illustrated by figure 4c. Where, ε_A and ε_D denote the strains at the reversal points A and D, respectively.

An integral and differential forms of the constitutive equation of stress component $\sigma_h(\varepsilon, \xi)$, along the

first or monotonous loading are, respectively:

$$\sigma_h(\varepsilon, \xi = 0) = g\ (\varepsilon) \qquad \text{and} \qquad \dot{\sigma}_h\ (\varepsilon, \xi = 0) = \frac{dg}{d\varepsilon}(\varepsilon)\ \ \dot{\varepsilon} \tag{4}$$

and during cyclic loadings:

$$\begin{array}{rl} & \Delta\sigma_h(\varepsilon, \xi) = g\ \{\Delta\varepsilon(\varepsilon, \xi)\} \\ \text{and} \qquad & \dot{\sigma}_h\ (\varepsilon, \xi)\ \equiv\ \Delta\ \dot{\sigma}_h\ (\varepsilon, \xi)\ =\ \frac{dg}{d\varepsilon}\{\Delta\varepsilon(\varepsilon, \xi)\}\ \ \dot{\varepsilon} \end{array} \tag{5}$$

where $g(\varepsilon)$ is a generic function, chosen for the polyamide strap behaviour, as follows:

$$g(\varepsilon) = \overset{\infty}{\sigma}_h\ \ th\{\ [2 - e^{-\ \frac{1}{2}\ (\delta\ \frac{\varepsilon}{\varepsilon^*})^2}]\ \frac{\varepsilon}{\varepsilon^*}\ \} \qquad \text{with} \qquad \varepsilon^* = \frac{\overset{\infty}{\sigma}_h}{E_h} \tag{6}$$

This generic function is defined by its modulus E_h and yield stress $\overset{\infty}{\sigma}_h$. A parameter δ could be chosen to change the shape of the function in the transition range (fig.5). With $\delta = 0$ relation 6 leads the function $g(\varepsilon)$ to a classic hyperbolic tangent. With $\delta > 0$, the radius of curvature in the transition range decreases if the value of δ increases. In the case of the polyamide straps, we chose $\delta = 1$, so the generic function $g(\varepsilon)$ is defined by two parameters, E_h and $\overset{\infty}{\sigma}_h$ only.
The behaviour of $\sigma_h(\varepsilon, \xi)$ defined as above is a special pure hysteresis model, because it does not take into account the Masing effect, like in the case of metallic materials for instance.

The viscoelastic stress component $\sigma_v(\varepsilon, \dot{\varepsilon})$ is obviously an important part of the behaviour of woven material. It is related to the amorphous phase of the polymer matter of the fibre, the widely viscoelastic behaviour of which is sensitive to the strain rate. The parameters of the behaviour of the stress component $\sigma_v(\varepsilon, \dot{\varepsilon})$ are an elastic modulus $E_v(\varepsilon)$ that could be a function of the current strain, and a steady state viscous stress $\overset{\infty}{\sigma}_v\ (\varepsilon, \dot{\varepsilon})$ that depends on strain rate and could also depend on the strain (fig. 3 and 4a), as follows:

$$\begin{array}{l} \overset{\infty}{\sigma}_v\ (\varepsilon, \dot{\varepsilon})\ =\ L(\varepsilon, \dot{\varepsilon})\ -\ J(\varepsilon) \\ E_v(\varepsilon)\ =\ (k_{ins}\ -\ 1)\ \frac{d}{d\varepsilon}\ J(\varepsilon) \end{array} \tag{7}$$

where k_{ins} is a constant parameter and $L(\varepsilon, \dot{\varepsilon})$, $J(\varepsilon)$ are two generic functions, which describe respectively the steady state at constant strain rate and the time-independent behaviour, during monotonous loading, such as:

$$\begin{array}{l} L(\varepsilon, \dot{\varepsilon})\ =\ \overset{\infty}{b}\ (\varepsilon).\log(\dot{\varepsilon} + \dot{\varepsilon}_0) +\ \overset{\infty}{a}\ (\varepsilon) \\ J(\varepsilon)\ = \lim_{\dot{\varepsilon}\ \to\ 0} L(\varepsilon, \dot{\varepsilon}) \end{array} \tag{8}$$

and $\overset{\infty}{a}\ (\varepsilon)$, $\overset{\infty}{b}\ (\varepsilon)$ are two analytical functions, such as:

$$\overset{\infty}{a}\ (\varepsilon)\ =\ \sigma_1.\exp(\frac{\varepsilon}{\varepsilon_1}) \qquad , \qquad \overset{\infty}{b}\ (\varepsilon)\ =\ b_0.\left[\left(\frac{\varepsilon}{\varepsilon_b}\right)^3 + 1\right]\ , \tag{9}$$

where σ_1, ε_1 and b_0, ε_b are constant parameters and $\dot{\varepsilon}_0 =\ 10^{-\frac{\sigma_1}{b_0}}$.

The viscoelastic stress component $\sigma_v(\varepsilon, \dot{\varepsilon})$ is described by a Maxwell-like constitutive differential equation:

$$\dot{\sigma}_v\ (\varepsilon, \dot{\varepsilon})\ =\ E_v(\varepsilon)\ \ \dot{\varepsilon}\ -\ \frac{E_v(\varepsilon)}{\eta(\varepsilon, \dot{\varepsilon})}\ \sigma_v(\varepsilon, \dot{\varepsilon}) \tag{10}$$

involving a viscosity parameter $\eta(\varepsilon, \dot{\varepsilon})\ =\ \overset{\infty}{\sigma}_v\ (\varepsilon, \dot{\varepsilon})\ /\ \dot{\varepsilon}$, defined from the steady state viscous stress.

The nonlinear elastic component $\sigma_r(\varepsilon)$ of semi-crystalline polymers is related mainly to their amorphous phase. Indeed the mechanical behaviour of amorphous polymers is strongly nonlinear elastic at the temperature and strain rate of their rubbery state (Tang et al., 2007). In the case of the woven

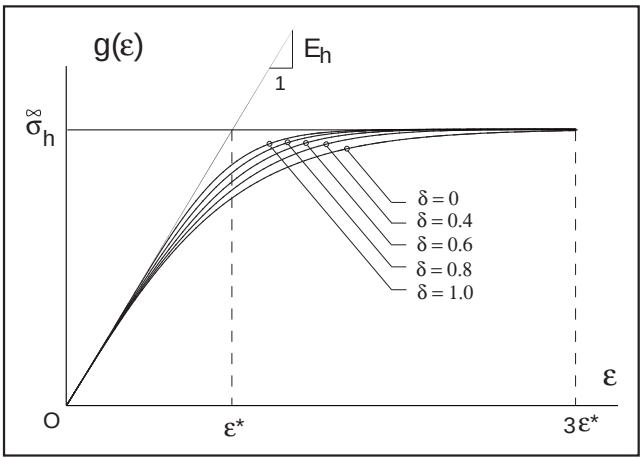

Figure 5: Generic function $g(\varepsilon)$ according to relation 6.

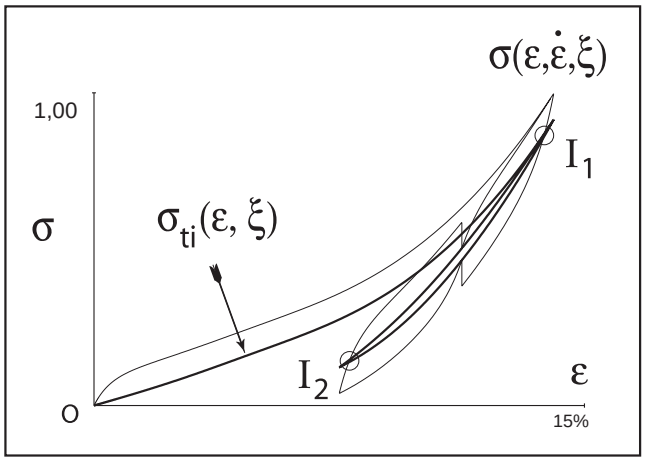

Figure 6: Time-independent stress $\sigma_{ti}(\varepsilon, \xi)$, which is the sum of $\sigma_h(\varepsilon, \xi)$ and $\sigma_r(\varepsilon)$ of figure 4.

materials made of stretched semi-crystalline polymer fibres, these effects are also caused by the high directing of the molecules of the amorphous phase to the fibre axis. This leads to a typical nonlinear reversible behaviour, with a very significant increase in the modulus at high values of strain. From the macroscopic point of view, the nonlinear elastic behaviour component is negligible when the strains are small, considering the physical origins of this behaviour. For this reason, at the strain equal to zero, we assumed the elastic modulus of the stress component $\sigma_r(\varepsilon)$ is also equal to zero (fig. 4b). The nonlinear elastic behaviour component $\sigma_r(\varepsilon)$ is described by a differential constitutive equation, such as:

$$\dot{\sigma}_r\ (\varepsilon)\ = E_r(\varepsilon)\ \dot{\varepsilon} \qquad \text{and} \qquad E_r(0) = 0 \tag{11}$$

and $E_r(\varepsilon)$ is defined as follows:

$$E_r(\varepsilon)\ =\ \frac{d}{d\varepsilon}\ J(\varepsilon)\ -\ \frac{d}{d\varepsilon}\ g(\varepsilon) \tag{12}$$

from the generic functions $g(\varepsilon)$ and $J(\varepsilon)$.

The visco-elasto-hysteresis model is completely defined by equations 1 to 12, involving seven constant parameters E_h, $\overset{\infty}{\sigma}_h$, k_{ins}, σ_1, ε_1, b_0 and ε_b.

3.2 Main properties of the visco-elasto-hysteresis model

3.2.1 Time-independent behaviour

The time-independent behaviour of the visco-elasto-hysteresis model corresponds to the case of infinitesimal strain (or stress) rate loadings. The viscoelastic stress component $\sigma_v(\varepsilon, \dot{\varepsilon})$ has a fluid behaviour and is the unique stress component that presents a time-dependent behaviour. Consequently according to the stress sum assumption 1, the time-independent behaviour is given by the superimposition of two stress components $\sigma_h(\varepsilon, \xi)$ and $\sigma_r(\varepsilon)$. This behaviour will be denoted by a time-independent stress component $\sigma_{ti}(\varepsilon, \xi)$ as:

$$\sigma_{ti}(\varepsilon, \xi) = \sigma_h(\varepsilon, \xi) + \sigma_r(\varepsilon) \tag{13}$$

The $\sigma_{ti}(\varepsilon, \xi)$ stress is reached by the total stress of the model at the ends of relaxation or creep periods. Indeed, during these periods the viscoelastic stress $\sigma_v(\varepsilon, \dot{\varepsilon})$ decreases to zero. Figure 6 illustrates this property on the example of loading of figure 4. The pure hysteresis stress component provides the time-independent behaviour with an irreversible character. If $\sigma_h(\varepsilon, \xi)$ is null, the time-independent behaviour becomes reversible and the visco-elasto-hysteresis model (fig. 3) is transformed into the viscoelastic *Zener* model. In the range of linear viscoelastic models, the time-independent behaviour is simply a

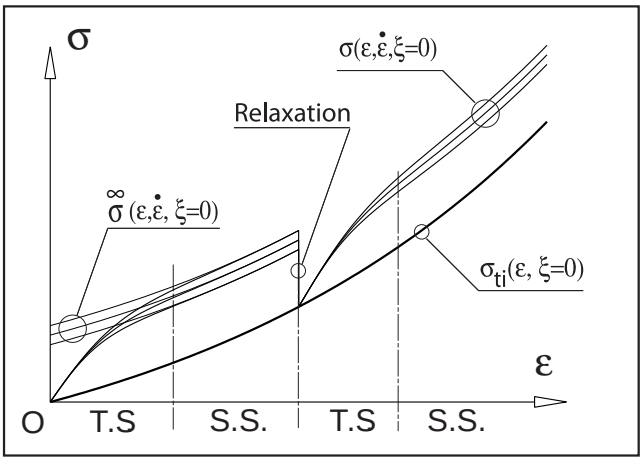

Figure 7: Transient state (T.S.) and steady state (S.S.) during monotonous loading.

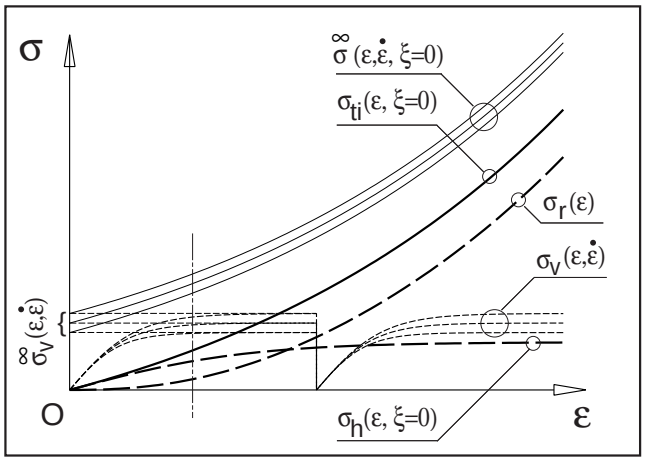

Figure 8: Diagram of superimposition assumption 1 in the case of a monotonous loading.

linear elastic behaviour $\sigma_{ti}(\varepsilon) = E_r\ \varepsilon$, with a constant modulus E_r, called *delayed elasticity*. The constitutive differential equation of the linear viscoelastic Zener model is:

$$\dot{\sigma} + \frac{\sigma}{\theta} \;=\; (E_v + E_r).\ \dot{\varepsilon} + \frac{E_r}{\theta}.\varepsilon \qquad \text{with} \qquad \theta = \frac{\eta}{E_v}\ . \tag{14}$$

where η is the viscosity parameter. This model has a solid behaviour, because its delayed elasticity is not null ($E_r \neq 0$). If the delayed elasticity of the Zener model is null ($E_r = 0$), it is the linear viscoelastic *Maxwell* model, the behaviour of which is of fluid type (Persoz, 1960).

Considering relations 11 and 13, elastic moduli of $\sigma_h(\varepsilon, \xi)$ and $\sigma_{ti}(\varepsilon, \xi)$ are the same at the beginning of the loading starting from the initial state of material ($\xi = 0$), (fig.4):

$$\lim_{\varepsilon \,\to\, 0} \frac{d\sigma_{ti}}{d\varepsilon}(\varepsilon, \xi = 0) = E_h \tag{15}$$

Taking into account the definition of visco-elasto-hysteresis model (§3.1), the time-independent behaviour during monotonous loading is described by the generic function $J(\varepsilon)$, such as:

$$\sigma_{ti}(\varepsilon, \xi = 0) \;=\; J(\varepsilon) = \overset{\infty}{a}\ (\varepsilon) - \frac{\sigma_1}{b_0}.\ \overset{\infty}{b}\ (\varepsilon)\ . \tag{16}$$

So, from previous relations 15 and 16, the modulus of pure hysteresis stress component is a function of parameters σ_1 and ε_1 :

$$E_h \;=\; \frac{\sigma_1}{\varepsilon_1}. \tag{17}$$

3.2.2 Steady state during monotonous loading at a constant rate

After sufficient time, during a loading at constant strain (or stress) rate, the transient state of the viscoelastic stress behaviour finishes and a steady state takes place. The steady state stress of the model is the total stress during this steady state at a constant rate. Figure 7 shows the sequence of the transient and steady states during a monotonous loading on the visco-elasto-hysteresis model. The transient state appears at the beginning of the loading starting from the initial state or after a long period of relaxation or creep. When the total stress $\sigma(\varepsilon, \dot{\varepsilon}, \xi = 0)$ reaches the steady state stress in monotonous loading $\overset{\infty}{\sigma}\ (\varepsilon, \dot{\varepsilon}, \xi = 0)$, the steady state begins. Figure 8 gives the evolution of stress components $\sigma_h(\varepsilon, \xi = 0)$, $\sigma_v(\varepsilon, \dot{\varepsilon})$, $\sigma_r(\varepsilon)$ and $\sigma_{ti}(\varepsilon, \xi = 0)$ during the monotonous loading of figure 7.

Considering relations 1 and 13, the steady state stress in monotonous loading $\overset{\infty}{\sigma}(\varepsilon, \dot{\varepsilon}, \xi = 0)$ is given as a function of the steady state viscous stress $\overset{\infty}{\sigma}_v(\varepsilon, \dot{\varepsilon})$ according to the following relation:

$$\overset{\infty}{\sigma}(\varepsilon, \dot{\varepsilon}, \xi = 0) \; = \overset{\infty}{\sigma}_v(\varepsilon, \dot{\varepsilon}) \; + \; \sigma_{ti}(\varepsilon, \xi = 0) \tag{18}$$

The generic functions $L(\varepsilon, \dot{\varepsilon})$ describes the steady state at constant strain rate during monotonous loading, by definition of visco-elasto-hysteresis model. Moreover, relations 7, 8, 16 and 18 indicate that in the case of an infinitesimal strain rate the total stress and its steady state stress $\overset{\infty}{\sigma}(\varepsilon, \dot{\varepsilon}, \xi = 0)$ are the same as the time-independent stress $\sigma_{ti}(\varepsilon, \xi = 0)$:

$$\begin{aligned} &\overset{\infty}{\sigma}(\varepsilon, \dot{\varepsilon}, \xi = 0) \; = \; L(\varepsilon, \dot{\varepsilon}) \\ \text{and} \qquad &\lim_{\dot{\varepsilon} \to 0} \overset{\infty}{\sigma}(\varepsilon, \dot{\varepsilon}, \xi = 0) \; = \; \sigma_{ti}(\varepsilon, \xi = 0) \end{aligned} \tag{19}$$

3.2.3 Instantaneous behaviour

The instantaneous behaviour of the visco-elasto-hysteresis model is a limit behaviour, which could be revealed for very short periods of time: at the beginning of a relaxation or creep period, just after a relaxation or creep period at the beginning of a constant rate reloading, just after a load reversal of a constant rate cyclic loading, during a high frequency cyclic loading with a little cycle amplitude, as a general rule just after a sudden changing of the mechanical loading condition. The parameter of the instantaneous behaviour of the visco-elasto-hysteresis model is an elastic modulus denoted here $E_{ins}(\varepsilon, \xi)$ as:

$$E_{ins}(\varepsilon, \xi) \; = \; E_v(\varepsilon) \; + \; E_r(\varepsilon) \; + \; \frac{d\sigma_h}{d\varepsilon}(\varepsilon, \xi) \tag{20}$$

This instantaneous modulus E_{ins} could depend on the current strain ε and on the reference memorized state ξ. In the case of linear viscoelasticity, the pure hysteresis component is null and their instantaneous behaviour is simply a linear elasticity, the instantaneous modulus of which is constant.

Definition 20 of instantaneous modulus and relation 13 lead to the following relation:

$$E_{ins}(\varepsilon, \xi) \; = \; E_v(\varepsilon) \; + \; \frac{d\sigma_{ti}}{d\varepsilon}(\varepsilon, \xi). \tag{21}$$

In the case of monotonous loading ($\xi = 0$), relations 7, 16 and 21 enabled us to derive the expression of instantaneous modulus:

$$E_{ins}(\varepsilon, \xi = 0) \; = \; k_{ins} \, \frac{d}{d\varepsilon} J(\varepsilon) \tag{22}$$

4 Experimental methods and results

4.1 Cyclic tensile tests

During these tests, the strain rate was maintained constant. At the load reversal of the cycles, the sign of the rate changed but its absolute value remained the same. The stress-strain loops were limited on the right by a given value of strain, and on the left by a given positive value of stress close to zero, so as to keep the tensile load and avoid any compression. Figure 9 gives a result of cyclic tensile test $oabcdefg$, which includes at its end a relaxation period gh. This result shows the particular *bean* shape of the stress-strain cycles often observed with woven materials.

4.2 Monotonous tensile tests at different strain rates

Monotonous tensile tests at constant strain rates were performed with straps of groups A and B. We tested the straps with strain rates ranging from $10^{-5}\ s^{-1}$ to $0,3\ s^{-1}$. Some tests were ended by a stress relaxation period at a constant strain. Figure 10 presents the stress-strain curves of monotonous tests

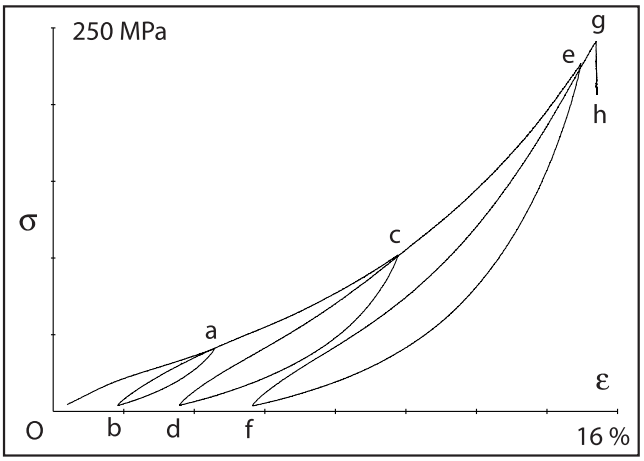

Figure 9: Result of cyclic tensile test $C35$ ($\dot{\varepsilon}$= $10^{-5}\ s^{-1}$).

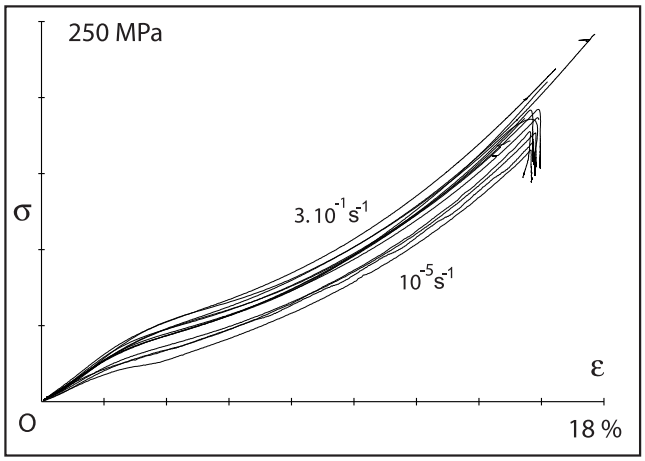

Figure 10: Results of monotonous tensile tests; the strain rates are from $10^{-5}\ s^{-1}$ to $3.10^{-1}\ s^{-1}$, the samples are from group A.

on straps from group A. These curves are composed of three zones; in the first zone the stress is less than $50\,MPa$, the second zone is between about 50 and $100\,MPa$ and the third zone presents stresses above $100\,MPa$. The transition between the first and the second zone is sharp and the transition between the second and third zone is very gradual.

Each stress-strain curve of a monotonous tensile test at a strain rate, like those in figure 10, is defined by at least 500 measurement points. This great number of points enabled us to present these experimental results in a stress versus strain rate graph at different strains. (fig. 11). For a given strain ε, the effect of strain rate on the stress is linear in a $\sigma - \log\dot{\varepsilon}$ diagram. This means that the viscous part of the behaviour of these polyamide straps is not linear; in the linear viscoelastic case, such curves are of an exponential type. Moreover, the strain rate sensitivity slope is not constant and depends on the strain value; this was observed in the case of the two groups of the straps. In other words, the viscosity parameter of this material is nonlinear and depends on current strain and strain rate.

We carried out linear regressions at different strains on $\sigma - \log\dot{\varepsilon}$ data; the dash-dotted lines on figure 11 are the regression lines. The solid lines are the same lines moved up and down on a distance equal to the regression standard deviation. At a given strain ε, the parameters of the regression line are its slope $b(\varepsilon)$ and its ordinate intercept point $a(\varepsilon)$, as follows:

$$\sigma(\varepsilon, \dot{\varepsilon}, \xi = 0) \;=\; b(\varepsilon).\log(\dot{\varepsilon}) \;+\; a(\varepsilon) \tag{23}$$

The evolutions of parameters $a(\varepsilon)$ and $b(\varepsilon)$ versus the strain are given in figures 12 and 13 respectively. Firstly, we noted that the behaviour of the two groups of straps can be distinguished in these figures. Indeed, the difference in behaviour is appreciable: it is higher than the dispersion amplitudes. In figure 13, at high strains, an increase in measures dispersion for the straps in group B is observed. This is due basically to the low number of measure points in this range of curve. Relation 23 and the evolutions of the parameters $a(\varepsilon)$ and $b(\varepsilon)$, given in figures 12 and 13, enabled us to get the whole characteristic features of the behaviour in monotonous tensile at different strain rates, for the two groups straps A and B. Mulliken and Boyce (2006) carried out uniaxial tension and compression tests on polycarbonate and PMMA amorphous polymers and obtained a similar stress evolution with respect to strain rate, close to a linear function of strain rate logarithm. Similarly, Bergström and Boyce (1998) presented an evolution of the stress, that *is proportional to the logarithm of the applied strain rate* and they remarked that *the proportionality constant increases with strain*, like the parameters $a(\varepsilon)$ and $b(\varepsilon)$ (fig. 12, 13).

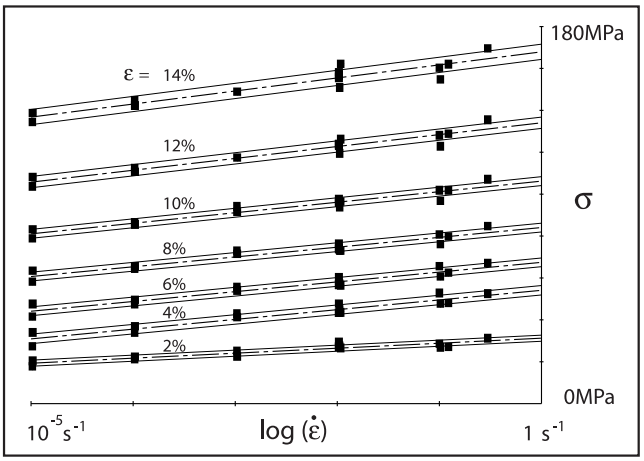

Figure 11: Stress versus strain rate for the straps from group A.

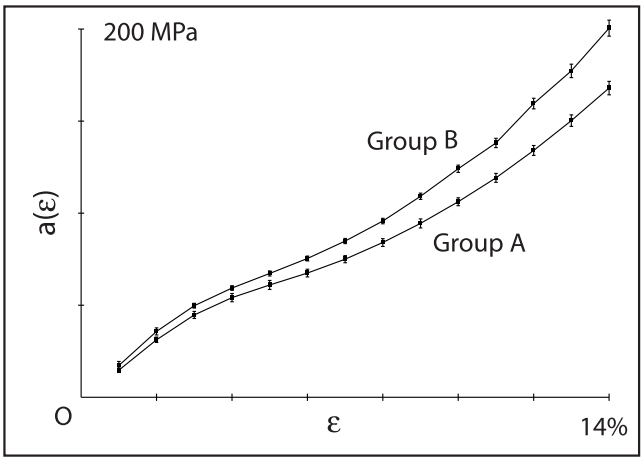

Figure 12: $a(\varepsilon)$ parameter as result of the linear regression, computed on the data of strap groups A and B. Above and below each point $a(\varepsilon)$ are shown the values of standard deviation.

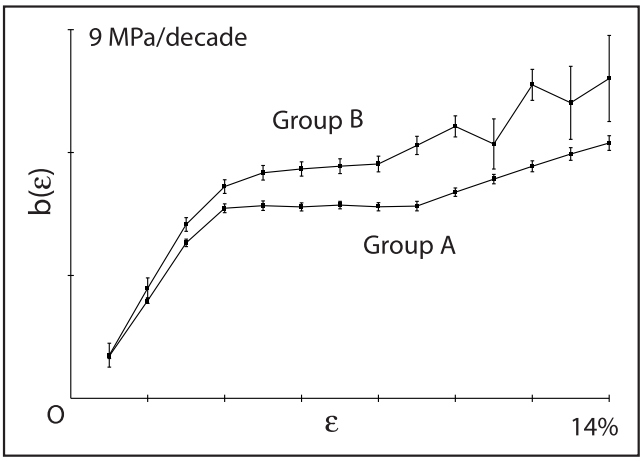

Figure 13: $b(\varepsilon)$ parameter as result of the linear regression, computed on the data of strap groups A and B. Above and below each point $b(\varepsilon)$ are shown the values of standard deviation.

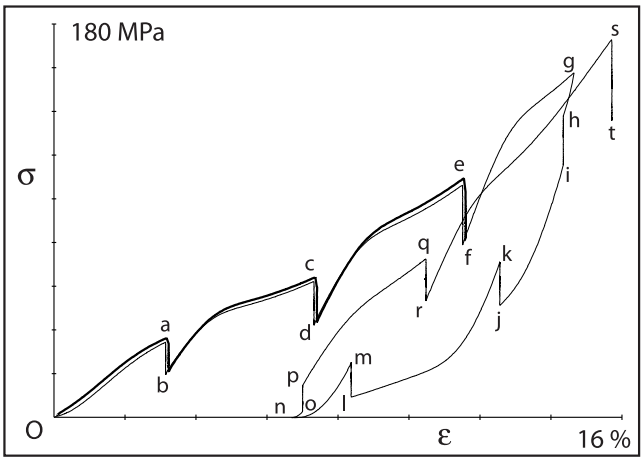

Figure 14: Results of two cyclic tensile tests with relaxation periods ($\dot{\varepsilon}$= 10^{-3} s^{-1}); $A37$ (bold line) and $A38$ (thin line).

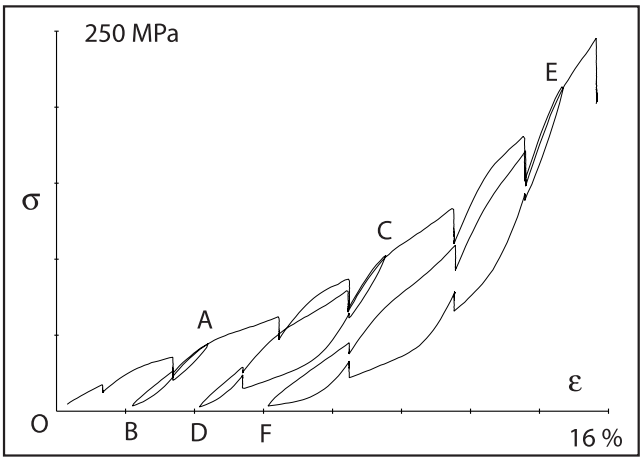

Figure 15: Result of cyclic tensile test $C36$ with relaxation periods ($\dot{\varepsilon}= 10^{-4}\ s^{-1}$).

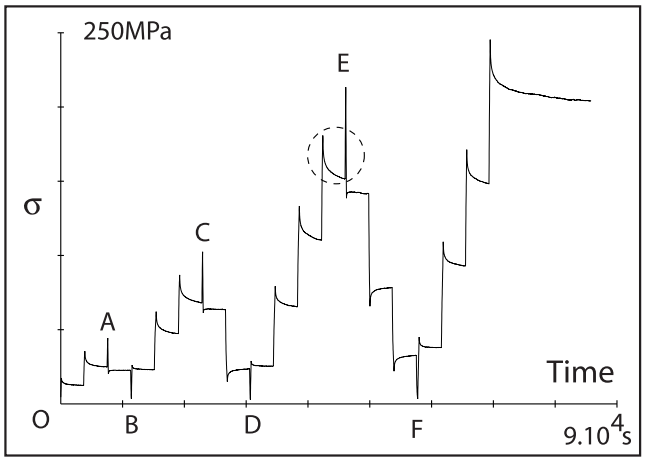

Figure 16: Stress versus time – test $C36$.

4.3 Cyclic tensile tests interrupted by relaxation periods

The strain rate of these tests was controlled and maintained constant during the loading and unloading processes. The results of three tests are given in figures 14 and 15. Test $A38$ presents one loading-unloading cycle (fig. 14), and three loading-unloading cycles were carried out during the test $C36$ (fig. 15). Test $A37$ was controlled at the same strain rate as $A38$, but presents no cycle, it is a monotonous tensile broken with relaxation periods. The same type of relaxation test is adopted by Lion (1997), Bergström and Boyce (1998), Khan and Lopez-Pamies (2002), Miehe and Göktepe (2005) and Diani et al. (2006) applied to rubbers.

During the relaxation stages, the stress may decrease or increase according to the location of the relaxation sequence in the stress-strain hysteresis loop. If the relaxation stage breaks a first or monotonous loading, the stress always decreases regardless of relaxation location. During the relaxation stages of test $C36$ (fig. 15), the stress decreases when the strain rate of the loading branch, which is broken due to relaxation, is positive, similar to during the first monotonous loading. But when the strain rate is negative, the stress increases during the relaxation stages, like during the ones of Bergström and Boyce (1998). Moreover, the stress relaxation amplitude seems to be lowest near and after a loading reversal point. The stress relaxation amplitude increases with the strain range between the last reversal point and the relaxation stage. Test $A38$ (fig. 14) shows that the stress relaxation amplitude could be null, if the relaxation stage breaks the loading branch at a special point. Indeed, the sign of variation of stress at a relaxation stage changes according to the location after the reversal point. Therefore, we may assume that a neutral point exists and corresponds to a relaxation stage, which is characterized by a stress amplitude vanishing to zero. This phenomenon is brought to the fore by relaxations hi and op in figure 14. Hence, the neutral points are located on the unloading branch between relaxations hi and jk, and on the reloading branch between relaxations op and qr.

During a reloading just after a relaxation period, the slope in the stress-strain graph is one of the highest. This slope increases with the value of deformation which characterizes the relaxation position (see for example branches bc and fg in figure 14). At a given relaxation strain, this slope seems to be constant whatever the mechanical history before: first loading, unloading or reloading (fig. 15).

Otherwise, the transient state just after a relaxation period presents a particular shape, like an overshoot above the steady state stress; firstly the stress rises linearly with the strain and soon beyond the steady state stress and then decreases in a second step and reaches this steady state stress.

Finally, figure 16 gives the time evolution of the stress during test $C36$. With this figure it is possible to observe what type of time evolution the stress has during the relaxation stages.

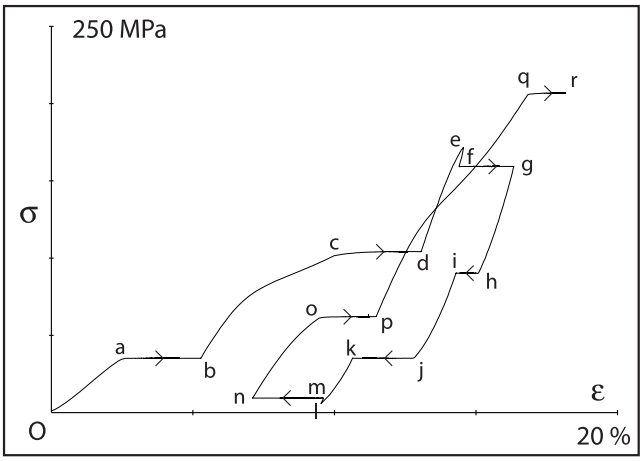

Figure 17: Result of cyclic tensile test $A36$ with creep periods ($\dot{\sigma}$= $32,9\,MPa/s$).

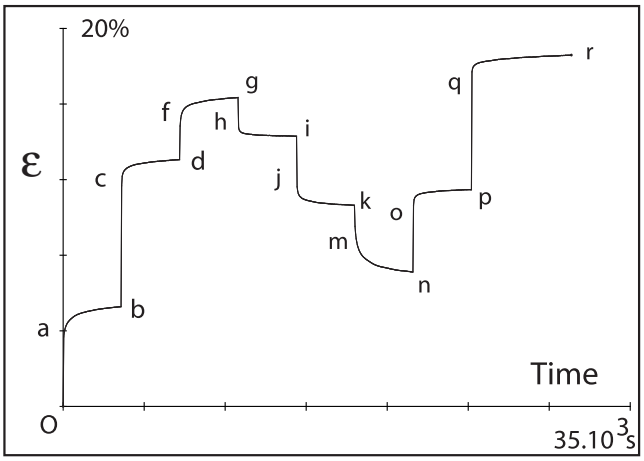

Figure 18: Strain versus time – test $A36$.

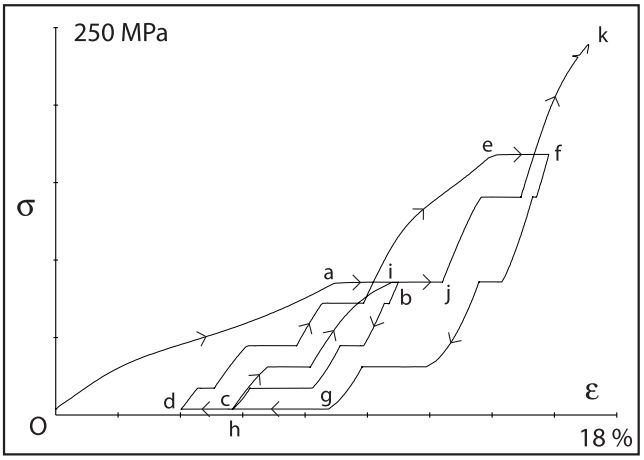

Figure 19: Result of cyclic tensile test $A14$ with creep periods ($\dot{\sigma}$= $6,6\,MPa/s$).

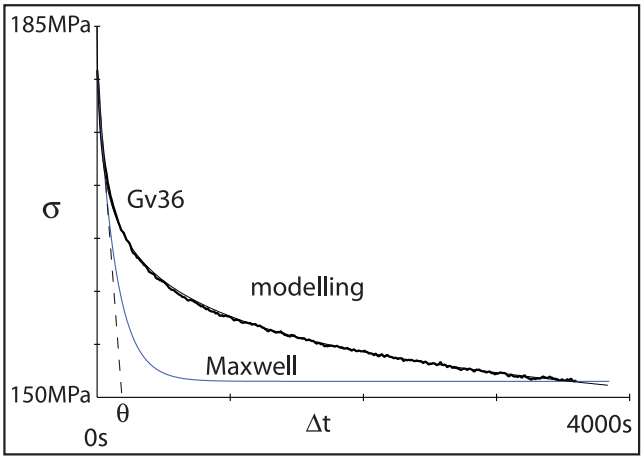

Figure 20: Comparison of a relaxation stress evolution of test $C36$ to the linear viscoelastic Maxwell model prediction and to a relaxation behaviour according to relation 24.

4.4 Cyclic tensile tests interrupted by creep periods

The stress rate of these tests was controlled and maintained constant. The loading, reloading and unloading processes were broken by some creep periods, during which the stress is constant. Two typical results are given in figures 17 and 19. One and two cycles were carried out during tests $A36$ and $A14$ respectively (fig. 17, 19). The evolution of strain during the creep stages is similar to the evolution of the stress during the relaxation stages; the sign of the strain variation during the creep periods depends on the location of the creep sequence stage in the hysteresis loop. Test $A36$ confirms the existence of a neutral point, on the stress-strain curve, corresponding to creep strain amplitude vanishing to zero; the material shows a no viscous behaviour at the neutral point (without creep). Indeed, figure 17 shows a change in the strain evolution direction during creeps fg and hi, and also during creeps mn and op.

In the same way as after the relaxation sequences, a reloading just after a creep period presents a special transient state with an overshoot, which is less pronounced than in the case of relaxation (see for example paths bc and pq in figure 17).

Figure 18 gives the time evolution of the strain during test $A36$. This figure allows us to observe the shape of the time evolution of strain during creep stages for strap material.

4.5 Relaxation and creep behaviour

Figure 20 gives a part of the time evolution of the stress during test $C36$. The relaxation stage extracted from the curve is seen in figure 16 and illustrated by a dashed circle. This relaxation stress evolution presents the typical shape of most relaxations whatever their location in the loading branch and the strain rate just before they occurred (Miehe and Göktepe, 2005; Drozdov and Christiansen, 2006; Khan et al., 2006).

The stress evolution, during a relaxation stage predicted by the classic linear viscoelastic Maxwell model, is also presented in figure 20; the Maxwell stress evolution is of an exponential type. The two parameters of the Maxwell model were calculated in order to take into account the whole variation of stress during the relaxation and the stress rate at the beginning of this relaxation period. The figure underscores a fundamental difference of stress curve shapes between the linear viscoelastic Maxwell model and test $C36$. The Maxwell stress evolution reaches its limit in a duration equal to three times its characteristic time θ. Whereas the $C36$ stress evolution decreases more and more slowly and does not show any threshold or asymptotic limit. This experimental stress evolution in a relaxation stage shows a typical shape that could be defined by a theoretical equation as follows:

$$\sigma(t) \;=\; -\,A\,.\,\log \Delta t \;+\; B\;, \tag{24}$$

where $A = 11,18\,MPa/_{\text{decade}}$, $B = 191,2\,MPa$. Figure 20 allows us to compare the experimental results with the basic relaxation model defined by relation 24; there is a good accordance between them.

The relaxation stress evolutions at the end of nine monotonous tensile tests on groups A and B (fig. 10), were studied. The strains at these relaxation stages are around 16%; the mean strain value is $\varepsilon = (15.8 \pm 0.1)\%$. The strain rates before these relaxations are from $10^{-5}s^{-1}$ to $10^{-1}s^{-1}$, and the duration of the relaxations are from $300s$ to $2h$. The mean value of the measurement of parameter A of relation 24, which defines the shape of the relaxation stress evolution, is:

$$A \;=\; 9,0 \;\pm\; 1,5\; MPa/_{\text{decade}} \qquad (95\%\, c.i.,\, n = 9)\;. \tag{25}$$

On these nine relaxation periods, the characteristic time θ was also measured. We observed that it is strongly dependent on the strain rate just before the relaxation stage. Assuming a linear function, we measured a slope in the $\log(\theta) - \log(\dot{\varepsilon})$ diagram:

$$\frac{d\log(\theta)}{d\log(\dot{\varepsilon})} \;=\; -0,743 \pm 0,025 \qquad (95\%\, c.i.,\, n = 9)\;, \tag{26}$$

Figure 18 gives the time evolution of creep strain during test $A36$. This figure suggests qualitatively that the type of time evolution of creep strain is similar to that of relaxation stress defined by relation 24.

5 Identification of visco-elasto-hysteresis model parameters

5.1 Steady state stress during monotonous tensile

This section deals with the material properties observed during the steady state in monotonous tensile. In order to leave out the transient state of $a(\varepsilon)$ and $b(\varepsilon)$ evolutions (fig. 12 and 13), we used the functions $\overset{\infty}{a}(\varepsilon)$ and $\overset{\infty}{b}(\varepsilon)$, which allow to define the steady state stress in monotonous tensile $\overset{\infty}{\sigma}(\varepsilon, \dot{\varepsilon}, \xi = 0)$ according to relations 8, 9 and 19. Figures 21 and 22 show the evolutions of $\overset{\infty}{a}(\varepsilon)$ and $\overset{\infty}{b}(\varepsilon)$ for the two groups of straps A and B. The identified values of parameters σ_1, ε_1, b_0 and ε_b, for the two groups of straps are given in table 2.

The significance of constant parameter $\dot{\varepsilon}_0$ for the two groups of the straps is shown in figure 23, where $\dot{\varepsilon}_0(A)$ and $\dot{\varepsilon}_0(B)$ are denoted respectively. Figure 24 presents the stress in monotonous tensile $\sigma(\varepsilon, \dot{\varepsilon}, \xi = 0)$ and the related steady state stress $\overset{\infty}{\sigma}(\varepsilon, \dot{\varepsilon}, \xi = 0)$ in the case of group A straps. In this figure, the monotonous tensile stress is not the measured raw data; this stress was calculated from relation 23 and the strain evolutions of coefficients $a(\varepsilon)$ and $b(\varepsilon)$ given in figures 12 and 13. The related steady state stress was calculated with relations 8, 9 and 19 and material parameters in table 2.

5.2 Time-independent stress in monotonous tensile

The time-independent stress in monotonous tensile $\sigma_{ti}(\varepsilon, \xi = 0)$ was calculated from relation 16 and material parameters in table 2. Figure 25 gives the obtained function $\sigma_{ti}(\varepsilon, \xi = 0)$ versus the strain, for group B straps. In the case of group A straps, figure 26 proposes a comparison between stress $\sigma_{ti}(\varepsilon, \xi = 0)$ as a result of relation 16 and the stress at the ends of relaxation and creep stages in monotonous loading. In this figure, there are two tests controlled with constant stress rates, $A14$ ($\dot{\sigma}$= 6,6 MPa/s) and $A36$ ($\dot{\sigma}$= 32,9 MPa/s) broken by creep periods, and two other tests controlled with constant strain rates, $A37$ and $A38$ ($\dot{\varepsilon}$= 10^{-3} s^{-1}) broken by relaxation periods. As a conclusion of this comparison, the time-independent stresses measured by the two different experimental methods are in accordance.

5.3 Modulus of the instantaneous behaviour

The first situation that the instantaneous behaviour appears in is the initial elasticity at the beginning of the first loading from the initial state of the material. Measurements of the initial elastic modulus were carried out for thirty-two tests on straps of groups A, B and C. No appreciable difference of values of initial modulus between these three types of straps was observed; therefore we grouped them as different measurements on a unique modulus. The result of these measurements of the initial elastic modulus, denoted E_0, is:

$$E_0 = 1,3 \pm 0,1\ GPa \qquad (95\%\, c.i.,\ n = 32)\ . \tag{27}$$

These measurements present a relatively significant dispersion. This is mainly due to experimental difficulties because a woven material does not have any rigidity in compression. The beginning of the tension is not clear and then the initial elastic behaviour is difficult to obtain. We noted that modulus E_0 does not seem to depend on the strain (or stress) rate of the tests.

At the beginning of the reloading just after relaxation and creep periods, the moduli of the instantaneous behaviour were measured. No difference in these measurements between the three types of straps was noticeable. The strain evolution of the instantaneous behaviour modulus along a monotonous loading $E_{ins}(\varepsilon, \xi = 0)$ is shown in figure 27. We noted that the measurements after relaxations and creeps and those of the initial modulus are in agreement and provide us with a characteristic evolution of $E_{ins}(\varepsilon, \xi = 0)$, which depends on the strain. In order to describe this evolution, we used relation 22, where k_{ins} is the only characteristic parameter. Obtained parameters k_{ins} for the two groups of straps A and B are given in table 2.

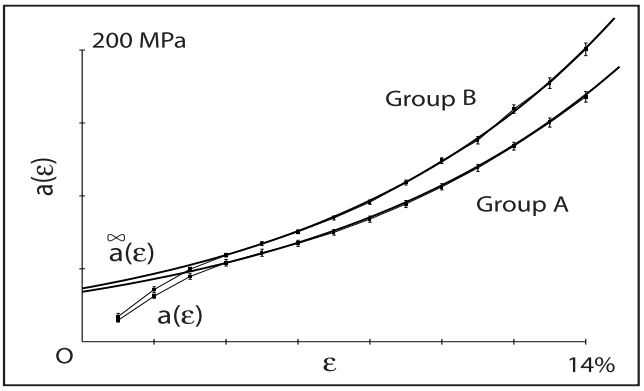

Figure 21: Strain evolution of coefficient $a(\varepsilon)$ and function $\overset{\infty}{a}(\varepsilon)$ computed with material parameters of table 2.

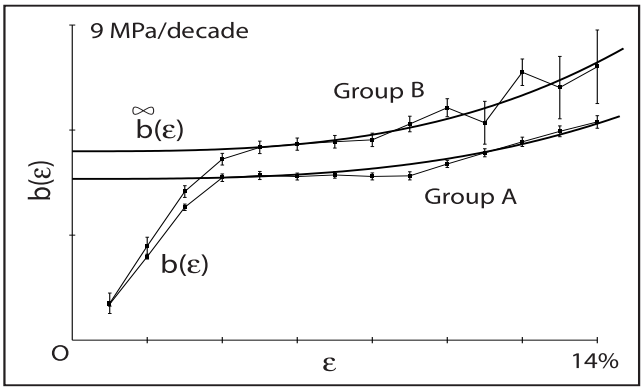

Figure 22: Strain evolution of coefficient $b(\varepsilon)$ and function $\overset{\infty}{b}(\varepsilon)$ computed with material parameters of table 2.

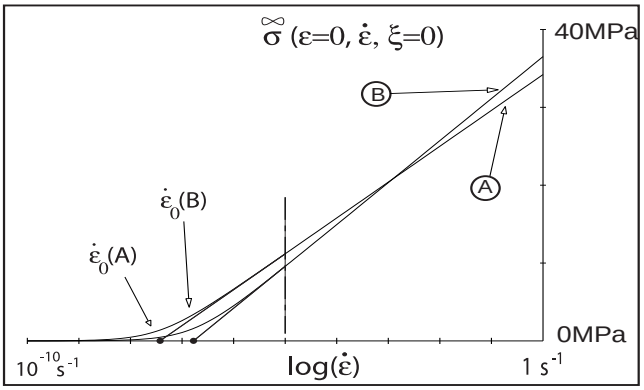

Figure 23: Steady state stress at a strain equal to zero and in monotonous tensile. Signification of parameter $\dot{\varepsilon}_0$ of relation 8.

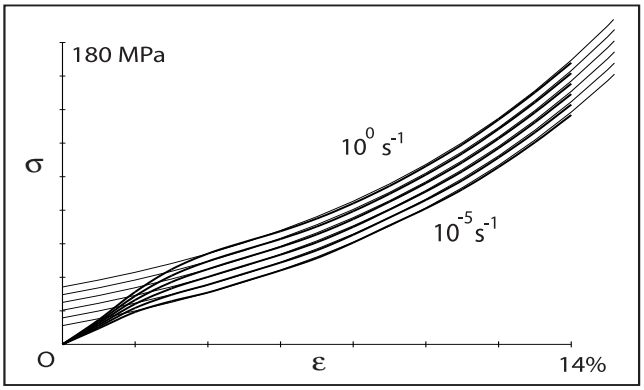

Figure 24: Stress in monotonous tensile $\sigma(\varepsilon, \dot{\varepsilon}, \xi = 0)$ (bold line) and related steady state stress $\overset{\infty}{\sigma}(\varepsilon, \dot{\varepsilon}, \xi = 0)$ (thin line) in the case of the group A straps.

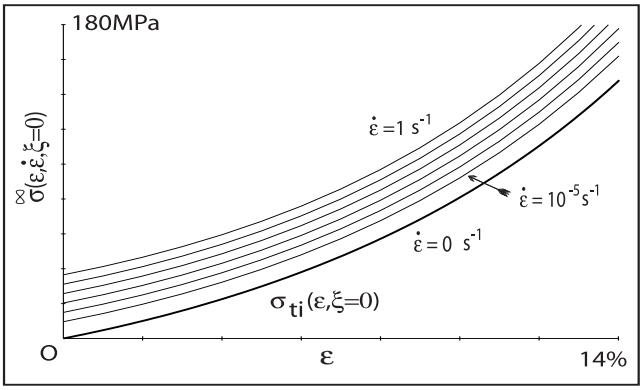

Figure 25: The steady state stress $\overset{\infty}{\sigma}(\varepsilon, \dot{\varepsilon}, \xi = 0)$ (thin line) and the time-independent stress $\sigma_{ti}(\varepsilon, \xi = 0)$ (bold line) for the group B straps.

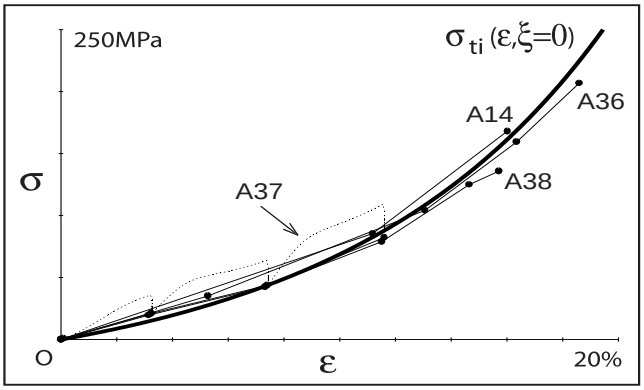

Figure 26: Comparison of the time-independent stress $\sigma_{ti}(\varepsilon, \xi = 0)$ computed by relation 16 and material parameters of table 2 (bold line) and the stress at the ends of relaxation and creep stages (thin line and bold points).

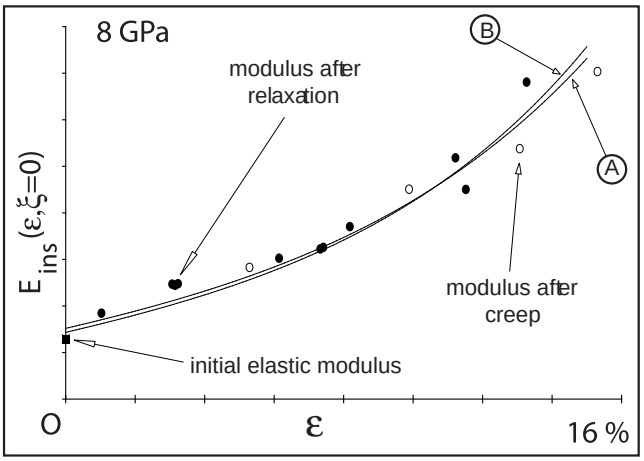

Figure 27: Instantaneous modulus in monotonous loading for the three groups of straps compared to curves A and B computed by relation 22 and material parameters of table 2.

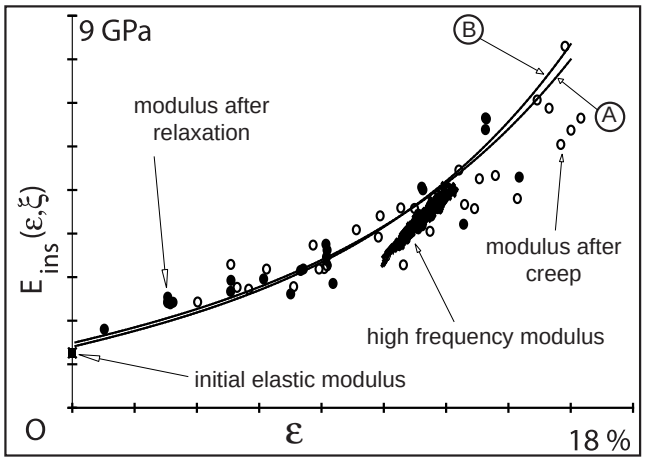

Figure 28: Instantaneous modulus in monotonous and cyclic loading for the three groups of straps compared to curves A and B computed by relation 22 and material parameters of table 2.

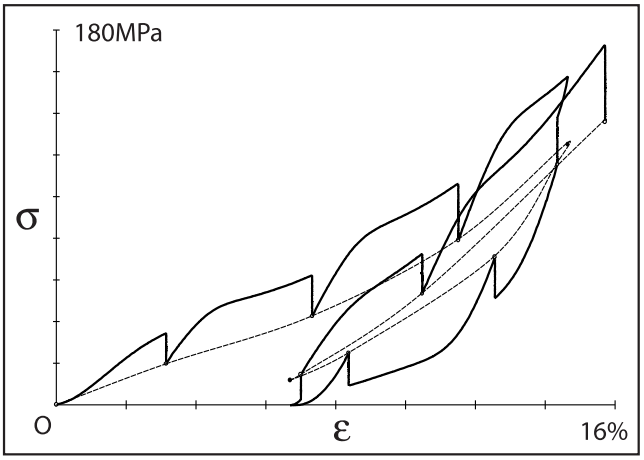

Figure 29: Estimated time-independent behaviour (dashed line) based on the state at the ends of the relaxation periods of test $A38$ (fig. 14).

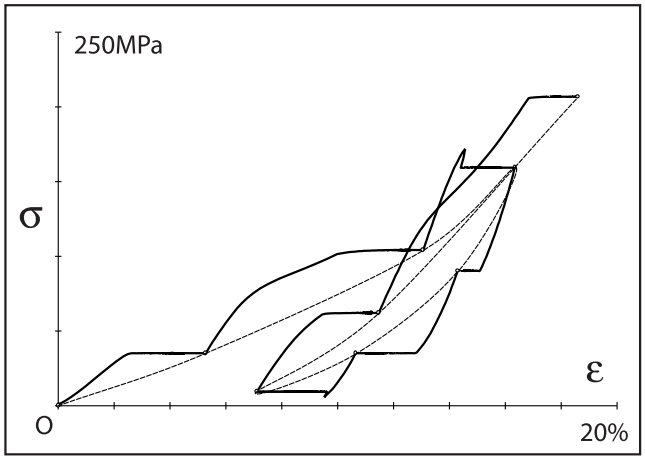

Figure 30: Estimated time-independent behaviour (dashed line) based on the state at the ends of the creep periods of test $A36$ (fig. 17).

The evolutions of $E_{ins}(\varepsilon, \xi = 0)$ described by relation 22 are also plotted in figure 27 and pointed out by the letters A and B, for the groups A and B of straps respectively. In figure 28, all other available measurements of $E_{ins}(\varepsilon, \xi)$, during monotonous and cyclic loading for the three types of the straps, were added to the data in figure 27. In figure 28, a measurement of a high frequency modulus was carried out during a sinusoidal loading at $8Hz$ frequency and $\Delta\varepsilon = \pm 0.6\%$ strain amplitude, with a group B strap. This figure shows that parameter ξ results in an increase in the dispersion of this measure. On this group of measures, it is not possible to distinguish the instantaneous behaviour in monotonous loading from the one in cyclic loading.

5.4 Pure hysteresis stress component

The stress component of pure hysteresis $\sigma_h(\varepsilon, \xi)$ is described by two parameters E_h and $\overset{\infty}{\sigma}_h$ (cf. § 3.1). Modulus E_h was obtained from relation 17 and the values of parameters σ_1 and ε_1, already identified (tab. 2).

Parameter $\overset{\infty}{\sigma}_h$ was obtained from the time-independent stress $\sigma_{ti}(\varepsilon, \xi)$ in cyclic loading, which could

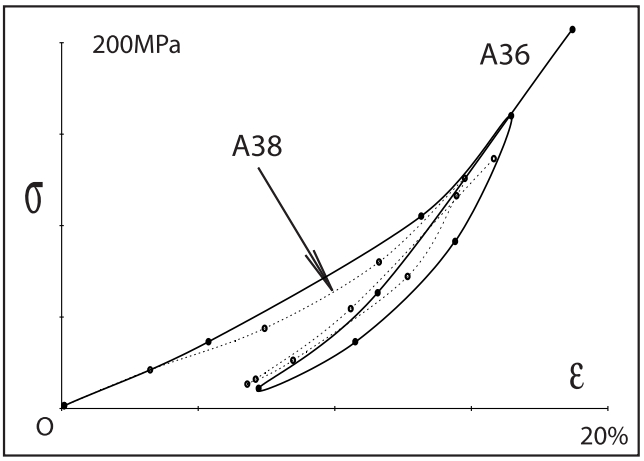

Figure 31: Time-independent stress $\sigma_{ti}(\varepsilon, \xi)$ measured by means of relaxation test $A38$ and creep test $A36$.

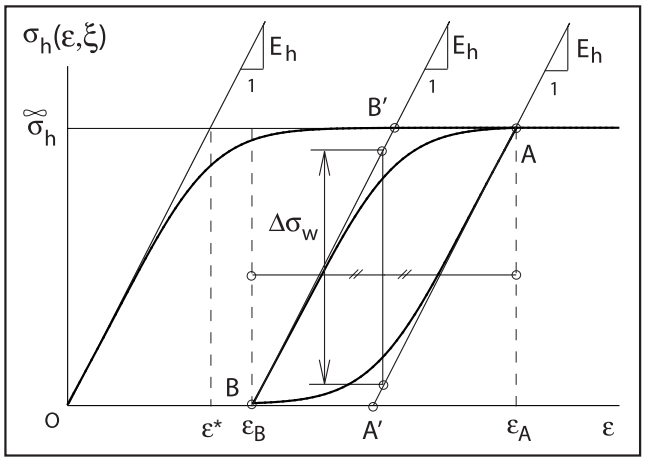

Figure 32: Method of measurement of the yield stress $\overset{\infty}{\sigma}_h$ of the pure hysteresis component.

be established by cyclic tensile tests broken by relaxation and creep periods. The time-independent behaviour may appear during these tests, if the duration of the relaxation or creep stages are long enough and if the number of relaxation and creep sequences is high enough along the loading branches. We performed the relaxation and creep periods with a mean duration of about one hour, and with a number of them ranging from two to six per hysteresis loop (for instance EF loop in figure 15). This choice was a compromise solution, between a realistic test duration, a most complete relaxation or creep of viscous effects and a sufficient number of measurement points to characterize the time-independent behaviour. Figures 29 and 30 give two typical results of $\sigma_{ti}(\varepsilon, \xi)$ obtained from test $A38$ (fig. 14) and test $A36$ (fig. 17) respectively. In the first figure, the stress $\sigma_{ti}(\varepsilon, \xi)$ is given by the σ-ε points at the ends of the relaxation periods. Such curves were performed by Lion (1997) applied to rubbers. In the second, the stress $\sigma_{ti}(\varepsilon, \xi)$ is given by the points at the ends of the creep periods. Figure 31 presents the $\sigma_{ti}(\varepsilon, \xi)$ established with these two tests. This figure allows us to compare the shape of the two unloading-reloading loops. Although these two experimental curves lack measure points, the behaviour during these two tests seems to be similar. As a general rule, we noted a good accordance between the $\sigma_{ti}(\varepsilon, \xi)$ measured with relaxation and creep tests, whatever the strain or stress rate of the loading. This result supports our assumption of stress superimposition (cf. relation 1).

The method of measurement of parameter $\overset{\infty}{\sigma}_h$ is based on the ordinate width of the hysteresis loops in $\sigma_{ti}(\varepsilon, \xi)$ versus ε diagram. This is illustrated in figure 32. Considering the lack of available measure points, we estimated the ordinate width of the loop AB by that of the parallelogram $AA'BB'$. This resulted in the following measure of $\overset{\infty}{\sigma}_h$:

$$\overset{\infty}{\sigma}_h = E_h\ (\varepsilon_A\ - \varepsilon_B)\ -\ \Delta\sigma_w. \tag{28}$$

with $\varepsilon_A\ - \varepsilon_B$ the strain amplitude of the loop AB and $\Delta\sigma_w$ the estimated stress width at the middle of the loop. Relation 28 can also apply to the time-independent component $\sigma_{ti}(\varepsilon, \xi)$ taking into account its definition given by relation 13. Consequently, relation 28 applied to the hysteresis loops of $\sigma_{ti}(\varepsilon, \xi)$ provided us with a measure of $\overset{\infty}{\sigma}_h$. Among the obtained measurement of $\overset{\infty}{\sigma}_h$, we could not distinguish one type of strap from another. The mean value for the three types of straps, is reported in table 2.

5.5 Viscoelastic stress component

The steady state viscous stress was determined by relations 7, 8 and material parameters in table 2. The resulting steady state viscous stress $\overset{\infty}{\sigma}_v\ (\varepsilon, \dot{\varepsilon})$ is presented as a function of the strain in figure 33

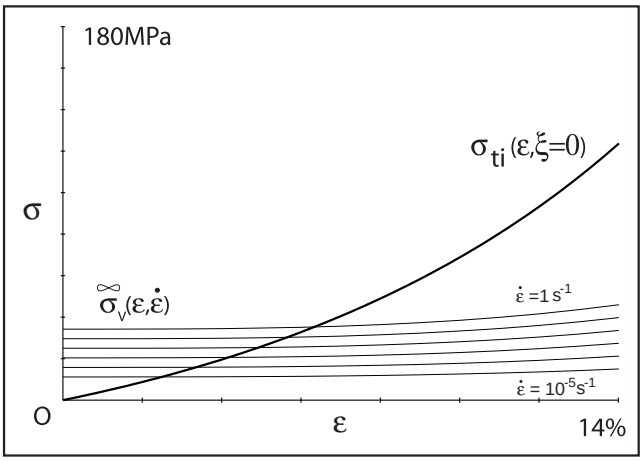

Figure 33: Steady state viscous stress $\overset{\infty}{\sigma}_v\ (\varepsilon, \dot{\varepsilon})$ (thin line) and time-independent stress $\sigma_{ti}(\varepsilon, \xi = 0)$ (bold line) for the group A straps.

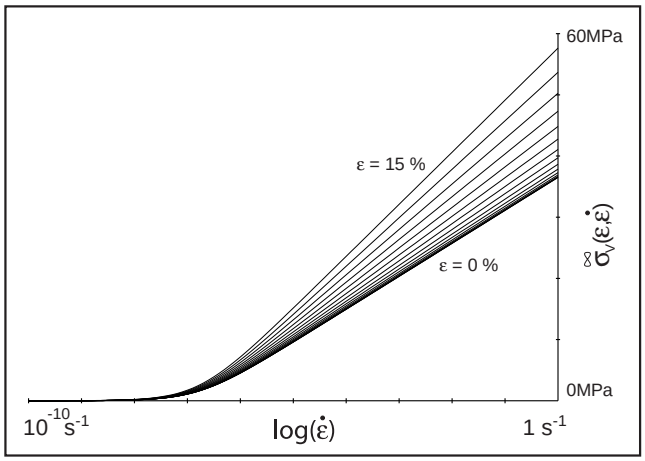

Figure 34: Steady state viscous stress $\overset{\infty}{\sigma}_v\ (\varepsilon, \dot{\varepsilon})$ as a function of the strain rate at different strains for the group B straps.

for the group A straps. The resulting steady state viscous stress is also presented as a function of the strain rate, for the group B straps in figure 34.

The steady state viscous stress $\overset{\infty}{\sigma}_v\ (\varepsilon, \dot{\varepsilon})$ does not present any saturation of the stress at the very high strain rates, as it did in the case of metallic materials (Bles et al., 2000b). The range of strain rate studied here is too low to conclude on this stress saturation at very high speed.

The elastic modulus $E_v(\varepsilon)$ of viscoelastic stress component was determined by relations 7, 8 and material parameters in table 2. The resulting elastic modulus $E_v(\varepsilon)$ is given in figure 35 for the two groups of straps A and B.

According to equations 7 and 22, the ratio of $E_v(\varepsilon)$ to $E_{ins}(\varepsilon, \xi = 0)$ depends only on parameter k_{ins}. This ratio is equal to 0.69 and 0.74 for the groups A and B of straps, respectively (tab. 2). Consequently, the greater part of the value of the instantaneous modulus, defined by relation 20, is due to elastic modulus $E_v(\varepsilon)$ of the viscous stress component. The sum of two other moduli represents a share of about 30% of $E_{ins}(\varepsilon, \xi = 0)$.

5.6 Reversible stress component

In the case of monotonous loading, relations 4 and 13 enabled us to obtain the reversible stress component $\sigma_r(\varepsilon)$:

$$\sigma_r(\varepsilon) \ = \ \sigma_{ti}(\varepsilon, \xi = 0) \ - \ g(\varepsilon). \tag{29}$$

Figure 36 illustrates this relation for the group B of straps. From relations 12 and 16 we can also determine modulus $E_r(\varepsilon)$:

$$E_r(\varepsilon) \ = \ \frac{d\sigma_{ti}}{d\varepsilon}(\varepsilon, \xi = 0) \ - \ \frac{dg}{d\varepsilon}(\varepsilon). \tag{30}$$

Figure 37 illustrates this relation in the case of the group B of straps.

Because of the definition of pure hysteresis component $\sigma_h(\varepsilon, \xi)$ given in section 3.1, modulus $\frac{d\sigma_h}{d\varepsilon}(\varepsilon, \xi)$ ranges from 0 to E_h whatever the value of ξ. This property is illustrated in the case of monotonous loading in figure 37. Table 2 shows that the value of modulus E_h is low by comparison with the value of instantaneous modulus $E_{ins}(\varepsilon, \xi)$ (fig. 28). Moreover, relation 20 points to the fact that the effect of parameter ξ on the instantaneous modulus is due to the term $\frac{d\sigma_h}{d\varepsilon}(\varepsilon, \xi)$. This explains the experimental difficulty to distinguish the influence of ξ in measurements of the instantaneous modulus during cyclic loadings, as was mentioned in section 5.3 (fig. 27 and 28).

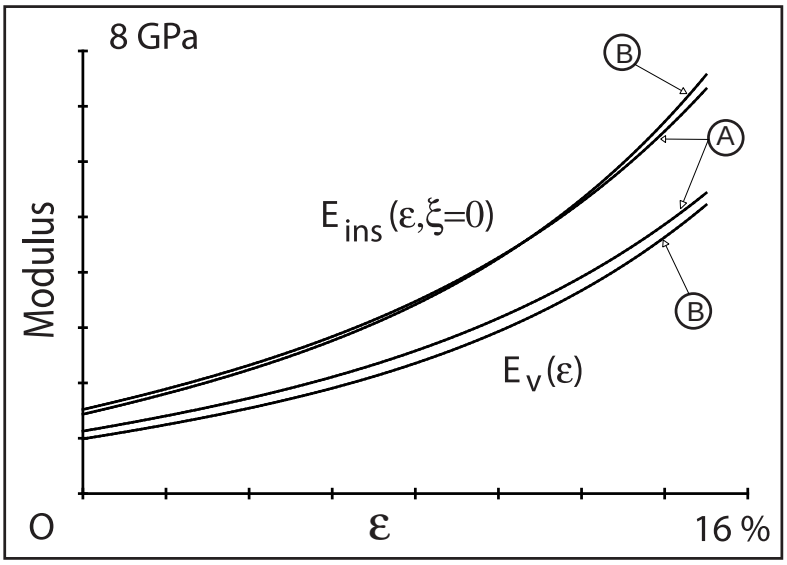

Figure 35: Elastic modulus $E_v(\varepsilon)$ of the viscoelastic component and instantaneous modulus in monotonous loading $E_{ins}(\varepsilon, \xi = 0)$, for the two groups of straps A and B.

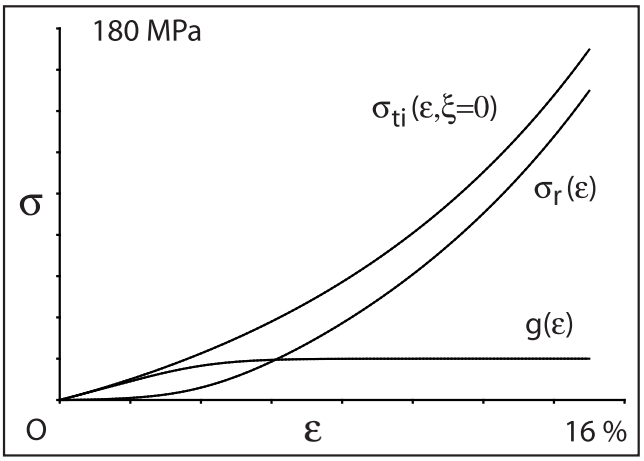

Figure 36: Time-independent stress $\sigma_{ti}(\varepsilon, \xi = 0)$ in monotonous loading and its splitting up into reversible stress $\sigma_r(\varepsilon)$ and pure hysteresis stress $g(\varepsilon)$ in monotonous loading, for the group B of straps.

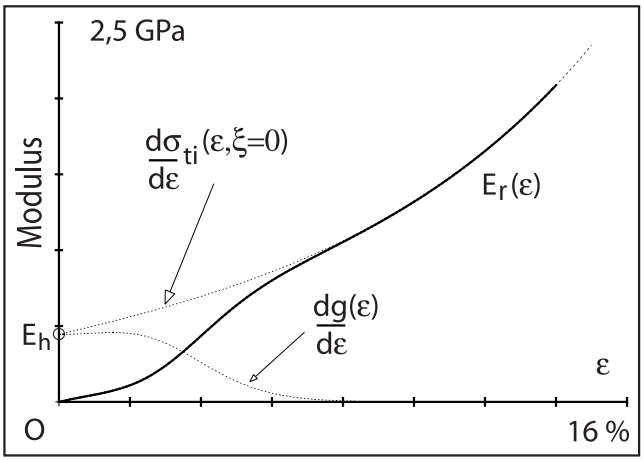

Figure 37: The splitting up of $\frac{d\sigma_{ti}}{d\varepsilon}(\varepsilon, \xi = 0)$ into the reversible and the pure hysteresis components, for the group B of straps.

Table 2: Identification of visco-elasto-hysteresis model parameters for the two groups of straps A and B.

Parameters	σ_1	ε_1	b_0	ε_b	k_{ins}	E_h	$\overset{\infty}{\sigma}_h$
Units	MPa	%	MPa/decade	%	–	MPa	MPa
Group A	34,21	8,75	4,60	20	3.89	391	18
Group B	36,51	8,20	5,39	18	3.22	445	

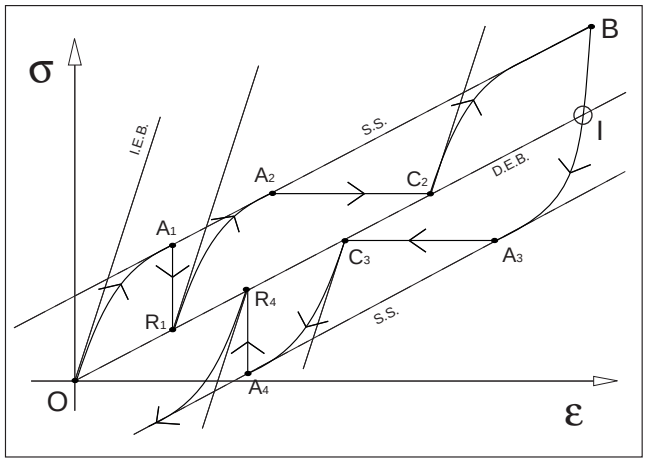

Figure 38: Linear viscoelastic behaviour during a loading and unloading at constant strain rate broken by relaxation (A_1R_1, A_4R_4) and creep (A_2C_2, A_3C_3) periods.

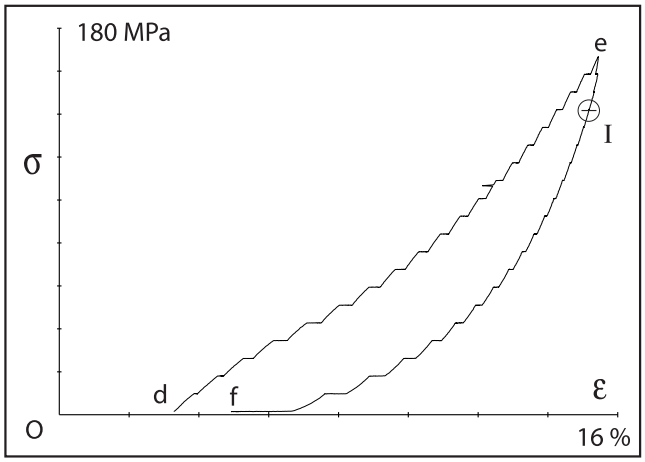

Figure 39: Result of test $A40b$ controlled at constant stress rate ($\dot{\sigma}= 1,3\,MPa/s$) and broken by a lot of creep periods of very short duration ($15s$).

6 Analysis of change in relaxation and creep orientations during cyclic loadings

The present section attempts to give an explanation for the phenomenon of direction change of relaxations and creeps in stress-strain hysteresis loops. This phenomenon is intricate, for this reason we will deal first with the simplest case of linear viscoelastic behaviour.

In theory, after a relaxation or creep stage of an infinite duration, the behaviour of a linear viscoelastic model reaches its delayed elastic behaviour (D.E.B.). The stress-strain point of this type of model reaches a point on behaviour D.E.B., whatever its location at the beginning of the relaxation or creep stage. We can consider a linear viscoelastic model in steady state (S.S.) at constant strain rate located at a given point A_i in the stress-strain diagram (fig. 38). During a relaxation and a creep stage starting from A_i, the stress-strain point moves to the points R_i and C_i respectively, on the dash-dotted line representing the different states of the delayed behaviour. The starting point A_i, could also be on the line representing the instantaneous elastic behaviour (I.E.B.) instead of the steady state. This case is the classic stress relaxation loading or creep loading with an Heaviside step loading of strain or stress, respectively (Persoz, 1960).

The direction of the relaxation or creep evolutions is given by the location of the starting point with respect to line D.E.B.. Because, during a relaxation or a creep stage, the stress-strain point of the linear viscoelastic model moves from the starting point directly to line D.E.B..

For instance, relaxation stages A_1R_1 and A_4R_4 show opposite stress evolutions ($\dot{\sigma}\leqslant 0$ and $\dot{\sigma}\geqslant 0$, respectively) because starting point A_1 of the first is above line D.E.B., while starting point A_4 of the latter is below this line. Similarly, creep stages A_2C_2 and A_3C_3 have opposite strain evolutions ($\dot{\varepsilon}\geqslant 0$ and $\dot{\varepsilon}\leqslant 0$, respectively).

Point I in figure 38, called the *neutral point*, at the intersection of the behaviour curve and line D.E.B. is particular; a relaxation or creep stage beginning at point I does not present any evolution of stress or strain. Moreover, the relaxation and creep stages that start at points between reversal point B and neutral point I have an evolution like those A_1R_1 and A_2C_2. Beyond neutral point I, the direction of the relaxation and creep evolutions changes, as in the case of A_3C_3 and A_4R_4.

The behaviour of the polyamide straps presented similar properties, albeit a little more complex. The delayed elastic behaviour of the linear viscoelastic models is in the case of the polyamide straps the time-independent behaviour: $\sigma_{ti}(\varepsilon, \xi)$ (fig. 6). We wondered if a neutral point exists for the behaviour of these straps. In this way, we carried out some cyclic tensile tests broken by a lot of creep periods of a very short duration ($15s$). Amin et al. (2006) performed akin tests called *multi-step* relaxation tests. Figure 39 gives a typical result; neutral point I is shown by a solid circle in unloading branch ef.

This neutral point is at the intersection of the total stress curve and the curve of time-independent stress component $\sigma_{ti}(\varepsilon, \xi)$ (points I_1 and I_2, fig. 6). While the delayed elastic behaviour of the linear viscoelastic model is linear and elastic, the delayed behaviour of the visco-elasto-hysteresis model is the time-independent behaviour that is neither linear nor elastic and presents a nonlinear character with hysteresis loops. Therefore, for the polyamide straps, the occurrence of the neutral point could be more intricate than in the linear viscoelastic case, but this point does exist, as we have seen in figure 39.

7 Conclusion

Sophisticated tensile tests were performed on polyamide fibre (PA66) woven strap samples, using a measurement of local deformation of woven material. Various monotonous and cyclic loadings, interrupted or not by relaxation and creep sequences, were carried out on a range of strain rates from 10^{-5} s^{-1} to 0.3 s^{-1}.

An analysis of experimental results was made through a visco-elasto-hysteresis model, based on the superimposition of three stress components of nonlinear viscoelastic, nonlinear elastic and elastoplastic types. Each of these constitutive stresses is related to a specific physical phenomenon that occurs during mechanical loading at the mesoscopic scale at the level of woven cell and/or at the microscopic scale at the level of fibre material. The complex visco-elasto-hysteresis behaviour of straps is characterized by its three essential behaviour properties: the steady state viscous stress as a function of strain and strain rate, the time-independent irreversible behaviour and the instantaneous modulus increasing with the strain. Based on these properties it is possible to characterize the three stress components of material visco-elasto-hysteresis behaviour: the pure hysteresis, the nonlinear viscoelastic and the nonlinear reversible stress components.

A coherent analysis of experimental results was proposed to understand and predict the change in relaxation and creep orientations during complex loading histories.

Acknowledgements

The authors would like to thank the *C.A.T.* (*Centre Aéroporté de Toulouse*) the Toulouse Airborne Center of the French Defence Procurement Agency *D.G.A.* (*Délégation Générale pour l'Armement*) for providing polyamide strap samples and for supporting this research programme.

References

Amin, A.F.M.S., Lion, A., Sekita, S., Okui, Y., 2006. Nonlinear dependence of viscosity in modeling the rate-dependent response of natural and high damping rubbers in compression and shear: experimental identification and numerical verification. International Journal of Plasticity 22, 1610-1657.

Averett, R.D., Realff, M.L., Michielsen, S., Neu, R.W., 2006. Mechanical behavior of nylon 66 fibers under monotonic and cyclic loading. Composites Science and Technology 66, 1671-1681.

Baesu, E., 2003. Finite deformations of elastic-plastic filamentary networks. International Journal of Non-Linear Mechanics 38, 1473-1479.

Baesu, E., 2007. A class of exact solutions for a 3D filamentary continuous medium. Computers and Mathematics with Applications 53, 317-323.

Banfield, S., Casey, N., 1998. Evaluation of fibre rope properties for offshore mooring. Ocean Engineering 25 (10) 861-879.

Beltran, J.F., Williamson, E.B., 2005. Degradation of rope properties under increasing monotonic load. Ocean Engineering 32, 826-844.

Bergström, J.S., Boyce, M.C., 1998. Constitutive modeling of the large strain time-dependent behavior of elastomers. Journal of the Mechanics and Physics of Solids 46 (5) 931-954.

Bles, G., Gadaj, S.P., Guelin, P., Nowacki, W.K., Tourabi, A., 2000. Thermomechanics of viscoplastic large strains of solid polymers. Arch. Mech. 52 (3) 397-427.

Bles, G., Nowacki, W.K., Tourabi, A., 2000. Viscoelastoplastic thermomechanical constitutive patterns at high rates of strain. J. Phys. 10 (Pr9) 27-32.

Bles, G., Gadaj, S.P., Nowacki, W.K., Tourabi, A., 2002. Experimental study of a PA66 solid polymer in the case of shear cyclic loading. Arch. Mech. 54 (2) 155-174.

Bles, G., 2002. Bases thermomécaniques de la modélisation du comportement des matériaux tissés et des polymères solides. Ph.D. Thesis, University Joseph Fourier of Grenoble, France.

Diani, J., Brieu, M., Vacherand, J.M., 2006. A damage directional constitutive model for Mullins effect with permanent set and induced anisotropy. European Journal of Mechanics A/Solids 25, 483-496.

Drozdov, A.D., Christiansen, J.deC., 2006. Constitutive equations for the nonlinear viscoelastic and viscoplastic behaviour of thermoplastic elastomers. International Journal of Engineering Science 44, 205-226.

Duhem, P.M., 1980. The evolution of mechanics (translated by M. Cole). Sijthoff and Noordhoff (English translation of "L'évolution de la mécanique", Paris 1903).

Fernandes, A.C., Rossi, R.R., 2005. Distorted polyester lines for model testing of offshore moored platforms. Ocean Engineering 32, 817-825.

Frank, G.J., Brockman, R.A., 2001. A viscoelastic-viscoplastic constitutive model for glassy polymers. International Journal of Solids and Structures 38, 5149-5164.

Ghoreishi, S.R., Cartraud, P., Davies, P., Messager, T., 2007. Analytical modeling of synthetic fiber ropes subjected to axial loads - Part I: A new continuum model for multilayered fibrous structures. International Journal of Solids and Structures 44, 2924-2942.

Holzapfel, G.A., Gasser, T.C., 2001. A viscoelastic model for fiber-reinforced composites at finite strains: Continuum basis, computational aspects and applications. Computer Methods in Applied Mechanics and Engineering 190, 4379-4403.

Kato, S., Yoshino, T., Minami, H., 1999. Formulation of constitutive equations for fabric membranes based on the concept of fabric lattice model. Engineering Structures 21, 691-708.

Khan, A.S., Lopez-Pamies, O., 2002. Time and temperature dependent response and relaxation of a soft polymer. International Journal of Plasticity 18, 1359-1372.

Khan, A.S., Lopez-Pamies, O., Kazmi, R., 2006. Thermo-mechanical large deformation response and constitutive modeling of viscoelastic polymers over a wide range of strain rates and temperatures. International Journal of Plasticity 22, 581-601.

King, M.J., Jearanaisilawong, P., Socrate, S., 2005. A continuum constitutive model for the mechanical behavior of woven fabrics. International Journal of Solids and Structures 42, 3867-3896.

Leech, C.M., 2002. The modelling of friction in polymer fibre ropes. International Journal of Mechanical Sciences 44, 621-643.

Lin, R.C., Schomburg, U., 2003. A finite elastic-viscoelastic-elastoplastic material law with damage: theoretical and numerical aspects. Computer methods in applied mechanics and engineering 192, 1591-1627.

Lion, A., 1997. On the large deformation behaviour of reinforced rubber at different temperatures. Journal of the Mechanics and Physics of Solids 45 (11/12) 1805-1834.

Lubarda, V.A., Benson, D.J., Meyers, M.A., 2003. Strain-rate effects in rheological models of inelastic response. International Journal of Plasticity 19, 1097-1118.

Miehe, C., Keck, J., 2000. Superimposed finite elastic-viscoelastic-plastoelastic stress response with damage in filled rubbery polymers - Experiments, modelling and algorithmic implementation. Journal of the Mechanics and Physics of Solids 48, 323-365.

Miehe, C., Göktepe, S., 2005. A micro-macro approach to rubber-like materials - Part II: The micro-sphere model of finite rubber viscoelasticity. Journal of the Mechanics and Physics of Solids 53, 2231-2258.

Mulliken, A.D., Boyce, M.C., 2006. Mechanics of the rate-dependent elastic-plastic deformation of glassy polymers from low to high strain rates. International Journal of Solids and Structures 43, 1331-1356.

Pargana, J.B., Lloyd-Smith, D., Izzuddin, B.A., 2007. Advanced material model for coated fabrics used in tensioned fabric structures. Engineering Structures 29, 1323-1336.

Persoz, B., 1960. Introduction à l'étude de la rhéologie. Dunod.

Spierings, A.B., Stämpfli, R., 2006. Methodology for the development of an energy absorber: Application to worker security ropes. International Journal of Impact Engineering 32, 1370-1383.

Tang, Y., Jiang, Z., Men, Y., An, L., Enderle, H-F., Lilge, D., Roth, S.V., Gehrke, R., Rieger, J., 2007. Uniaxial deformation of overstretched polyethylene: In-situ synchrotron small angle X-ray scattering study. Polymer 48, 5125-5132.

Tourabi, A., Guelin, P., Favier, D., 1995. Towards modelling of deformable ferromagnets and ferro-electrics. Arch. Mech. 47 (3) 294-323.

Tourabi, A., Guelin, P., Favier, D., Nowacki, W.K., 1997. From material discrete memory patterns to the study of demagnetization-like processes. Arch. Mech. 49 (4) 737-766.

Xue, P., Peng, X.Q., Cao, J., 2003. A non-orthogonal constitutive model for characterizing woven composites. Composites: Part A 34, 183-193.